



A dynamic multi-level model for adsorptive solar cooling

Giulio Santori^{a,*}, Alessio Sapienza^b, Angelo Freni^{b,1}

^a Università degli Studi e-Campus, Via Isimbardi 10, 22060 Novedrate, Como (CO), Italy

^b CNR-ITAE, Istituto di Tecnologie Avanzate per l'Energia 'Nicola Giordano' S. Lucia sopra Contesse, 98126 Messina, Italy

ARTICLE INFO

Article history:

Received 3 July 2011

Accepted 24 November 2011

Available online 17 December 2011

Keywords:

Solar cooling
Adsorption
Dynamic model
Silica gel
Refrigeration
Spectral analysis

ABSTRACT

This paper focuses on the development of a dynamic multi-level model for simulating of a solar cooling system adopting an adsorption chiller. The model integrates detailed simulation of the adsorption cycle (component level) into the transient simulation of the solar cooling system (system level). The chiller investigated was a standard two bed silica gel/water unit. The model was used to ascertain the feasibility of solar-driven adsorption cooling and for optimization purposes. In the base case simulated, the adsorption chiller cooled down the outdoor air to 16.1 °C. The daily average COP of the chiller was 0.18. Consequently, a spectral analysis was performed on these data for identification of the correlation among the variables involved in the solar cooling system in order to study the effects of the input parameters on the outputs. The outcomes were that the COP depends mainly on $T_{ev} > Q_{cond} > Q_{cool} > Q_{heat}$ and the thermal power delivered to the hot storage unit correlates $T_{z1} > T_c$.

© 2011 Elsevier Ltd. All rights reserved.

1. Introduction

Vapor compression refrigeration systems demand large quantities of electrical energy and involve mechanical parts in motion. The sustainability of using synthetic refrigerants is also an issue. On the other hand, adsorption refrigeration systems need low-temperature thermal energy to perform a thermodynamic cycle and they do not need a compressor, reducing electrical energy consumption. Adsorption refrigeration systems also have the advantages of being environment-friendly, as water can be used as working fluid having no ozone depletion or global warming potential. Adsorption refrigeration technologies driven by waste heat or renewable energy have thus attracted interest in recent years [1,2]. The technologies are still under development but few commercial products are ready in the market [3–5]. Studies have been conducted on numerous adsorption systems driven by solar energy, focusing mainly on machines using silica gel and water because they have a relatively low regeneration temperature (<100 °C) [6–8]. Field tests have shown that silica gel adsorption chillers can be efficiently operated using a solar energy source [9].

Different theoretical models have been proposed to describe the chiller's operation [5,10–13]. The earlier models presented the response of the machine operating in steady-state conditions for

few successive cycles [13]. More recently, a model was proposed for predicting the behavior of a silica gel/water chiller by studying the functioning of numerous successive cycles in terms of dynamic heating conditions, condensation and evaporation, which revealed a good agreement with experimental data [5]. To characterize the machine in transient conditions, theoretical studies were performed [10,11] in which various time-dependent functions (linear, sinusoidal, step, pulse) were applied to the temperature of the heat carrier fluid for desorption. The development of these models has shown that:

- 1) It is difficult to generalize on the machine's behavior for a given plant setting;
- 2) The start-up transient, up until the machine reaches a steady-state, must be thoroughly investigated;
- 3) The management of the machine's internal logic (end-phase conditions) needs to be accurately studied in order to optimize the COP in variable weather conditions.
- 4) A slow response to changes in the input data may occur, which makes it difficult to quantify the effect of the parameters on the chiller's operation [12];
- 5) The machine must be inserted in a realistic hydraulic context, with the consequent problem of controlling the evolution of a large number of parameters;
- 6) The machine's management, during the start-up transient and in the passage between the chiller's operating stages, must be optimized when the conditions of the external hydraulic loops are not stationary and predictable.

* Corresponding author. Tel.: +39 071 2204636; fax: +39 071 2204770.

E-mail addresses: giulio.santori@uniecampus.it (G. Santori), alessio.sapienza@itaecnr.it (A. Sapienza), angelo.freni@itaecnr.it (A. Freni).

¹ Tel./fax: +39 09 0624296.

To address these issues is necessary improving previous models and a deeper analysis of derived data. This means developing mathematical models with two main features:

- 1) Dynamic: capable of processing weather data input that varies in time;
- 2) Multi-level [14]: able to follow the evolution of the main quantities in the single subsystems (adsorption machine, storages, air treatment unit, etc.) and contemporary the solar cooling system, to perform black box type or detailed considerations;

The present work describes a dynamic multi-level model for assessing the performance of an adsorption chiller and its interactions with a realistic solar-powered setting. The two main parts into which the model can be divided are described separately below. Finally a spectral analysis of the data is proposed in order to estimate the correlations among the variables and the climatic data.

2. Plant description (base case)

Fig. 1 shows the layout of the solar cooling system for air conditioning. It consists of an adsorption chiller (rated 3 kW) operating with four heat exchangers for the condensation, evaporation and ad/desorption of two beds. The considered adsorption chiller was similar to the chiller reported in [15]. The heat of condensation and adsorption are dissipated by a remote dry cooler (rated 8 kW). The evaporator is used to produce the cooling effect by providing refrigerated water. The chiller is connected to two thermal storage units for managing the peak cooling demand and thermal availability. Both the storage units are stratified in three overlapping layers. The hot storage unit (2400 L) is powered by a field of flat solar thermal collectors (40 m²) and a backup boiler (rated 30 kW). The cold storage unit (900 L) serves an air treatment unit (ATU). The ATU takes outdoor air (0.2 m³/s) and treats it in cooling and dehumidification, adiabatic mixing and post-heating sections. For the solar collector field, the feed pump is operated

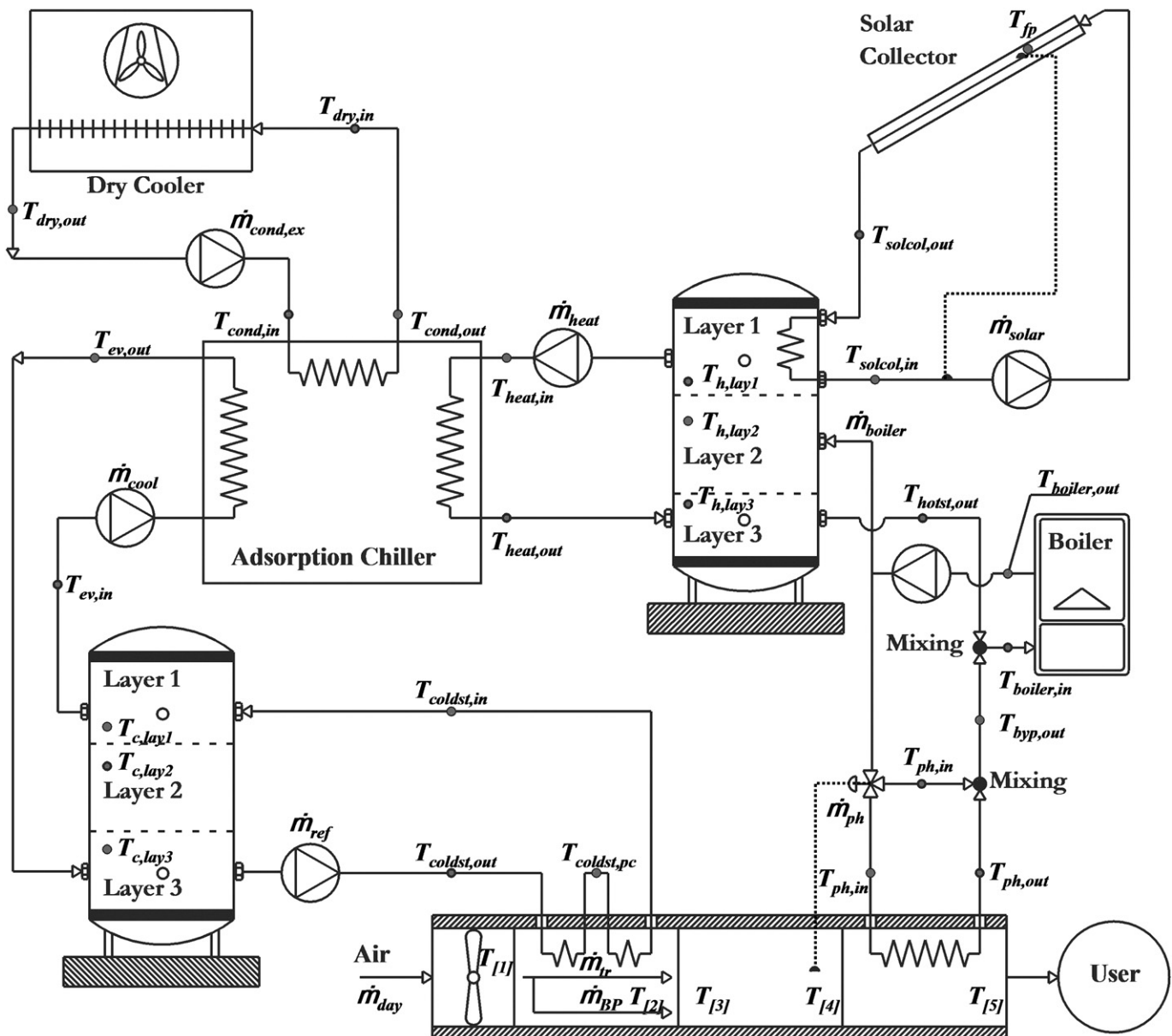


Fig. 1. Diagram of the process and instrumentation at the plant.

just when the temperature of the lower layer in the hot storage unit ($T_{h,lay3}$) is lower than the mean temperature of the solar collector field plates (T_{fp}). All the components are operated from 9.00 to 19.00 h, except for the solar collector field which is activated independently.

3. The input data

The climatic data for the town of Ancona, Italy were acquired hourly. The data available were the average values of global radiation (horizontal plane), ambient temperature and relative humidity. Data were acquired from 1 June 2007 to 30 August 2007. The radiation data were adjusted to give the global radiation on a plane tilted at 30° [16]. Then the data were statistically processed to obtain a single day representative of the summer period. Each hourly data outside the 99.5% confidence interval were excluded. The hourly means were calculated on the remaining values, to obtain one representative day for each month considered so obtaining three days. The three days was averaged obtaining a single day which was repeated three times, determining the set of climatic data input. Fig. 2 shows the trends of the solar radiation, temperature and relative humidity as input for the model.

4. The adsorption chiller model

The unit involved in this study is a two bed, silica gel-water adsorption chiller with no regeneration. Even though the previously proposed multi-bed regenerative and re-heated chillers show higher performance [17,18] this basic configuration was adopted to avoid introducing effects on the results relating to the type of machine, and thereby obtain more general information. The following assumptions were stated:

- 1) The adsorbent was always in equilibrium with the adsorbate
- 2) The gaseous phase behaves as an ideal gas
- 3) The properties of the solid and the gaseous phase are assumed constant
- 4) All the thermal losses are negligible

The mathematical system describing the operation of the chiller is summarized in by Eqs. (1)–(5). The indices for the eqs. from (1) to (5) are given in Table 1. Since the equations recurring at each stage are very similar and the model of the plant as a whole contains a very large number of equations, it seemed preferable to present

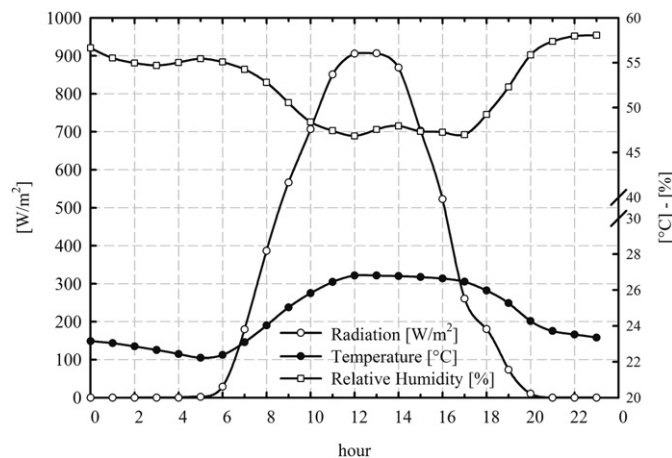


Fig. 2. Trend of climatic data for the fictitious day.

Table 1

End of phase conditions and indexing for Eqs. (1)–(5).

	Ph. I	Ph. II	Ph. III	Ph. IV
α	heat	heat	dry	Dry
β	cond	cond	ev	Ev
γ	c	c	ev	Ev
σ	cond	cond	ev,ex	ev,ex
μ	heat	heat	ev,ex	ev,ex
δ	0	1	0	1
End of phase conditions				
Thermodynamic ^a	$p_z > p_c$	$T_z > T_{sup}$	$p_z > p_{ev}$	$T_z > T_{inf}$
Temporal ^b	$t_{end,1}$	$t_{end,2}$	$t_{end,3}$	$t_{end,4}$

^a The temperature T_{sup} is calculated as the sum of the temperature at the start of the phase plus ΔT_{sup} (Table 3); the temperature T_{inf} is calculated as the difference, i.e. the temperature at the start of the phase less ΔT_{inf} (Table 3); the pressures at the end of phases 1 and 3 are the saturation pressures at the water condensation and evaporation temperatures, respectively.

^b $t_{end,1,2,3,4}$ are calculated from the sum of the phase start time plus a fixed Δt (Table 3).

them in compact form. Thus, by following the indexing in Table 1, we can track the energy and mass balances for each phase. Energy and mass balance in the adsorption machine (considering one bed) is:

$$\begin{aligned} (M_z C_{z,eq} + M_{z,ex} C_{z,ex}) \frac{dT_z}{dt} - M_z \Delta H_{ads} \frac{dw}{dt} \delta \\ = U_{z,ex} A_{z,ex} (T_{\alpha,in} - T_{\alpha,out}) \end{aligned} \quad (1)$$

The energy balances of the packed bed heat exchanger (Eq. (16)) and for the water inside the machine (Eq. (17)) are:

$$T_{\alpha,out} = T_z + e^{-\frac{A_{z,ex} U_{z,ex}}{m_{\alpha} c_{pw}}} (T_{\alpha,in} - T_z) \quad (2)$$

$$M_z \frac{dw}{dt} L_w = -U_{\beta,ex} A_{\beta,ex} (T_{\gamma} - T_{\beta,ex}) \delta - c_{\beta,ex} m_{\beta,ex} \frac{dT_{\beta,ex}}{dt} \delta \quad (3)$$

The energy balances for the water in the evaporator and condenser (machine side Eq. (18), plant side Eq. (19)):

$$\begin{aligned} M_{\beta,ex} c_{\beta,ex} \frac{dT_{\beta,ex}}{dt} = U_{\beta,ex} A_{\beta,ex} (T_{\gamma} - T_{\beta,ex}) \delta + \dot{m}_{\beta,ex} c_{pw} \\ (T_{\beta,in} - T_{\beta,out}) \delta \end{aligned} \quad (4)$$

$$T_{\beta,out} = T_{\beta,ex} + e^{-\frac{A_{\beta,ex} U_{\beta,ex}}{m_{\beta} c_{pw}}} (T_{\beta,in} - T_{\beta,ex}) \quad (5)$$

Auxiliary equations needed to solve the system are given in the Appendix. Fig. 3 shows the chiller circuit in the various phases of the process and how the fluid flows are diverted during the different phases.

The equations to solve are enabled or disabled according to the succession of phases in Fig. 3. It was consequently implemented a control system that not only determines the right sequence of the phases for each bed, but also guarantees the proper offsetting of the thermodynamic cycles of the two beds. The two conditions for enabling the passage from one phase to the other are:

- 1) Thermodynamic condition: when certain temperature and pressure conditions are reached (Table 1).
- 2) Temporal condition: the maximum time allowable to complete a phase; if the thermodynamic condition is not met, the phase changes anyway after a certain preset time interval (Table 1).

Table 1 details the thermodynamic and temporal conditions for each phase in the thermodynamic cycle.

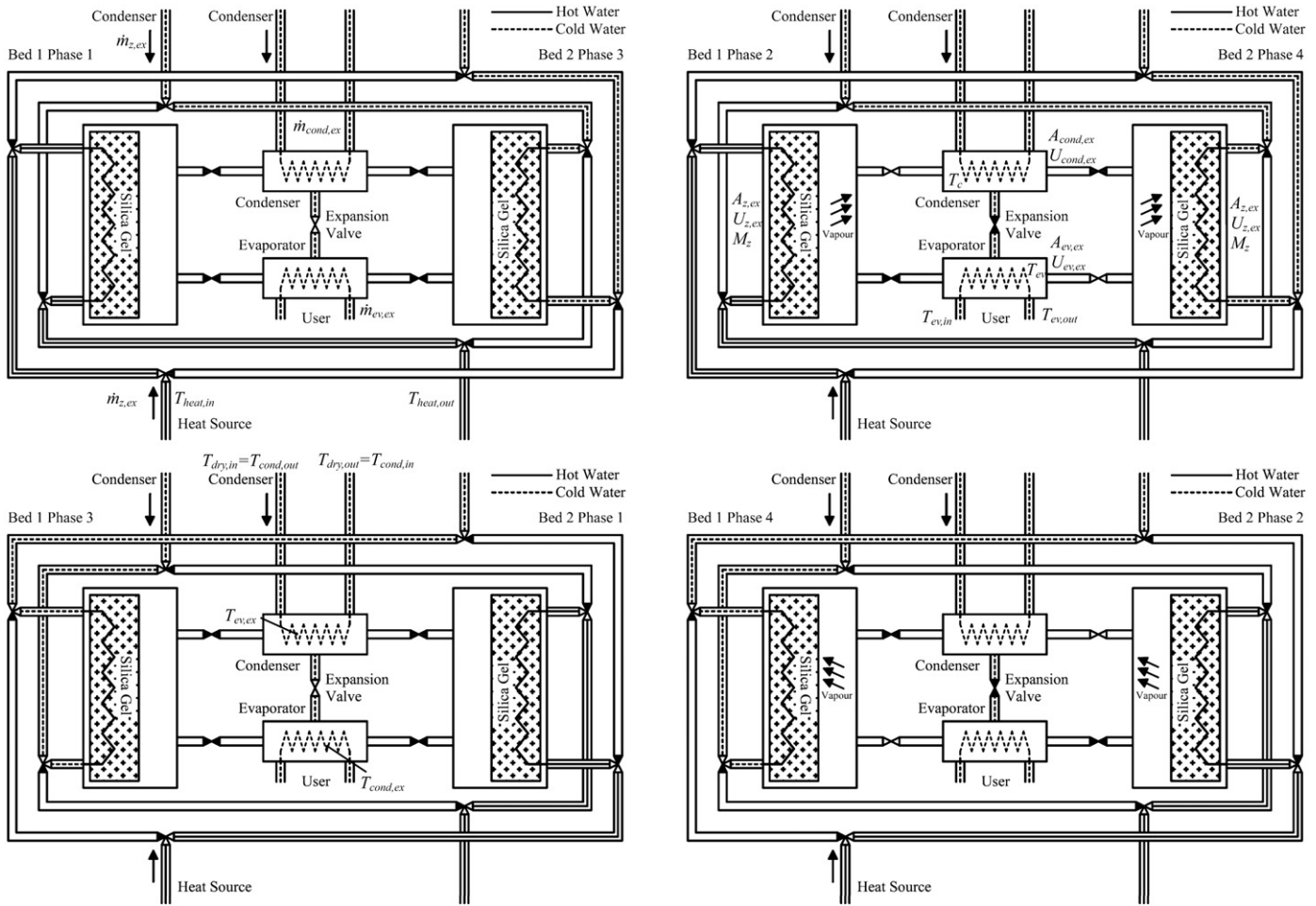


Fig. 3. Chiller phases.

If only one bed satisfies the thermodynamic condition, such bed waits until the thermodynamic condition or the temporal condition of the other bed is met. On the other hand, if one of the two beds satisfies the temporal condition, the phase transition is allowed even if the other bed has not satisfied the thermodynamic or temporal condition. The thermodynamic condition thus functions as an AND type of logical gate, the temporal as an OR type of logical gate.

The logic for differentiated variables initialization was a fundamental aspect to run the model. About such logic the values used for initializing the variables on the first and on subsequent days during the start-up transient were different. For a limited number of variables, for the days after the first, the ambient temperature was taken as initializing temperature, in other cases the last temperatures of the previous simulated day was taken.

Finally the values of T_{ev} and T_c were obtained from the two beds following the logic of the phases. The value of T_{ev} or T_c was thus read from one bed or the other, depending on which bed is active.

5. The plant model

The study of the solar cooling system demands the mathematical description of the loops involved and the storage units, therefore the use of several variables in addition to those concerning the chiller's operation. Apart from the adsorption chiller, the other systems involved in the plant are shown in Fig. 1.

The mathematical equations of the plant were implemented based on the following assumptions:

- 1) Negligible internal temperature gradients in every component (except the storage units);
- 2) Air was considered as an ideal gas;
- 3) The specific heat and density of the air and water were assumed to be constant within the operating temperature range;

The governing equations are listed in Table 2. The model is useful both for drawing general conclusions and for more detailed considerations on each subsystem of the plant.

The storage units were assumed to consist of three overlapping layers and the ATU of sections for cooling, dehumidification, adiabatic mixing and post-heating. In the ATU the outside air is taken at ambient conditions and subsequently treated according to the straight line of the ambient thermal factor until the dew point where dehumidification begins. Successively the air is sent for adiabatic mixing and post-heating. Then it is released into a user-room. This section operates between 9.00 and 19.00 h.

However this multi-level approach demands the introduction of control systems to harmonize the operation of the subsystems and to make the start-ups and shut-downs consistent. This means implementing a logic to reinitialize the differentiated variables according to their value at a previous point in time.

Table 2

Equations governing the solar cooling system.

Energy and mass balances in the ATU. Cooling (Eqs. (9)–(12)), dehumidification (Eqs. (13), (14)), adiabatic mixing (Eqs. (15)–(17)), post-heating (Eqs. (18)–(20)):

$$\varepsilon \dot{m}_{tr} c_{pa} (T_{[1]} - T_{coldst,out}) = \dot{m}_{tr} [c_{pa} (T_{[1]} - T_{[2]}) + r (x_{[1]} - x_{[2]})] \quad (9)$$

$$RFe \dot{m}_{tr} c_{pa} (T_{[1]} - T_{coldst,out}) = \dot{m}_{tr} c_{pa} (T_{[1]} - T_{[2]}) \quad (10)$$

$$\dot{m}_{tr} [c_{pa} (T_{[1]} - T_{[2]}) + r (x_{[1]} - x_{[2]})] = \dot{m}_{ref} c_{pw} (T_{coldst,pc} - T_{coldst,out}) \quad (11)$$

$$x_{[R]} = x_{[1]} - ((x_{[1]} - x_{[2]}) (T_{[1]} - T_{[R]})) / (T_{[1]} - T_{[2]}) \quad (12)$$

$$\varepsilon \dot{m}_{tr} c_{pa} (T_{[R]} - T_{coldst,out}) = \dot{m}_{tr} [c_{pa} (T_{[R]} - T_{[3]}) + r (x_{[R]} - x_{[3]})] \quad (13)$$

$$\dot{m}_{tr} [c_{pw} (T_{[R]} - T_{[3]}) + r (x_{[R]} - x_{[3]})] = \dot{m}_{ref} c_{pw} (T_{coldst,in} - T_{coldst,pc}) \quad (14)$$

$$\dot{m}_{air,day} = \dot{m}_{tr} + \dot{m}_{BP} \quad \text{with} \quad \dot{m}_{BP} = BP \dot{m}_{air,day} \quad (15)$$

$$\dot{m}_{air,day} x_{[4]} = \dot{m}_{tr} x_{[3]} + \dot{m}_{BP} x_{[1]} \quad (16)$$

$$\dot{m}_{air,day} H_{[4]} = \dot{m}_{tr} H_{[3]} + \dot{m}_{BP} H_{[1]} \quad (17)$$

$$\dot{m}_{ph,in} c_{pw} (T_{ph,in} - T_{ph,out}) = \dot{m}_{day} c_{pa} (T_{[5]} - T_{[4]}) \quad (18)$$

$$x_{[5]} = x_{[4]} \quad (19)$$

$$\dot{m}_{ph,in} c_{pw} (T_{ph,out} - T_{ph,in}) = U_{ph,ex} A_{ph,ex} \Delta T_{lm,ph} \quad (20)$$

Energy balances in the mixing points downstream from the post-heating exchanger (Eq. (21)) and before the boiler inlet (Eq. (22)):

$$\dot{m}_{ph} c_{pw} T_{byp,out} = (\dot{m}_{ph} - \dot{m}_{ph,in}) c_{pw} T_{ph,in} + \dot{m}_{ph,in} c_{pw} T_{ph,out} \quad (21)$$

$$(\dot{m}_{boiler} + \dot{m}_{ph}) c_{pw} T_{boiler,in} = \dot{m}_{boiler} c_{pw} T_{hotst,out} + \dot{m}_{ph} c_{pw} T_{byp,out} \quad (22)$$

Solar collector (Eqs. (23) and (24)), boiler (Eq. (25)) and dry cooler (Eq. (26)) energy balances:

$$\dot{M}_{fp} c_{fp} \frac{dT_{fp}}{dt} = (\tau \alpha)_{eff} I_{tilt} A_{coll} - \dot{m}_{solar} c_{pw} (T_{solcol,out} - T_{solcol,in}) - U_{fp/Amb} A_{fp/Amb} (T_{fp} - T_{Amb}) \quad (23)$$

$$U_{fp} A_{fp} \Delta T_{lm,fp} = \dot{m}_{solar} c_{pw} (T_{solcol,in} - T_{solcol,out}) \quad (24)$$

$$T_{boiler,out} = T_{boiler,in} + (Q_{boiler} / P_{boiler}) \quad (25)$$

$$T_{dry,in} = T_{Amb} + (T_{dry,out} - T_{Amb}) e^{-((U_{dry} A_{dry}) / (c_{pw} (\dot{m}_{cond,ex} + \dot{m}_{z,ex})))} \quad (26)$$

Energy balances in the cold (Eqs. (27)–(30)) and hot water (Eqs. (31)–(35)) storage units:

$$V_{c,lay1} c_{pw} \rho_w \frac{dT_{c,lay1}}{dt} = \dot{m}_{ref} c_{pw} (T_{coldst,in} - T_{c,lay1}) + \dot{m}_{ev,ex} c_{pw} (T_{c,lay2} - T_{c,lay1}) + U_{coldst} A_{c,lay1} (T_{Amb} - T_{c,lay1}) + U_w A_{c,lay} (T_{c,lay2} - T_{c,lay1}) \quad (27)$$

$$V_{c,lay2} c_{pw} \rho_w \frac{dT_{c,lay2}}{dt} = \dot{m}_{ref} c_{pw} (T_{c,lay1} - T_{c,lay2}) + \dot{m}_{ev,ex} c_{pw} (T_{c,lay3} - T_{c,lay2}) + U_{coldst} A_{c,lay2} (T_{Amb} - T_{c,lay2}) + U_w A_{c,lay} [(T_{c,lay1} - T_{c,lay2}) + (T_{c,lay3} - T_{c,lay2})] \quad (28)$$

$$V_{c,lay3} c_{pw} \rho_w \frac{dT_{c,lay3}}{dt} = \dot{m}_{ref} c_{pw} (T_{c,lay2} - T_{c,lay3}) + \dot{m}_{ev,ex} c_{pw} (T_{ev,out} - T_{c,lay3}) + U_{coldst} A_{c,lay3} (T_{Amb} - T_{c,lay3}) + U_w A_{c,lay} (T_{c,lay2} - T_{c,lay3}) \quad (29)$$

$$T_{ev,in} = T_{c,lay1}; T_{coldst,out} = T_{c,lay3} \quad (30)$$

$$V_{h,lay1} c_{pw} \rho_w \frac{dT_{h,lay1}}{dt} = \dot{m}_{solar} c_{pw} \Delta T_{lm,h,lay1} + \dot{m}_{heat} c_{pw} (T_{c,lay2} - T_{h,lay1}) + U_{hotst} A_{h,lay1} (T_{Amb} - T_{h,lay1}) + U_w A_{c,lay} (T_{c,lay2} - T_{h,lay1}) \quad (31)$$

$$V_{h,lay2} c_{pw} \rho_w \frac{dT_{h,lay2}}{dt} = \dot{m}_{boiler} c_{pw} (T_{boiler,out} - T_{h,lay2}) + \dot{m}_{heat} c_{pw} (T_{c,lay3} - T_{h,lay2}) + U_{hotst} A_{h,lay2} (T_{Amb} - T_{h,lay2}) + U_w A_{h,lay} [(T_{h,lay3} - T_{h,lay2}) + (T_{c,lay1} - T_{h,lay2})] \quad (32)$$

$$V_{h,lay3} c_{pw} \rho_w \frac{dT_{h,lay3}}{dt} = \dot{m}_{heat} c_{pw} (T_{heat,out} - T_{h,lay3}) + U_{hotst} A_{h,lay3} (T_{Amb} - T_{h,lay3}) + U_w A_{h,lay} (T_{h,lay2} - T_{h,lay3}) \quad (33)$$

$$\dot{m}_{solar} c_{pw} (T_{solcol,out} - T_{solcol,in}) = U_{stsolcol,ex} A_{stsolcol,ex} \Delta T_{lm,h,lay1} \quad (34)$$

$$T_{hotst,out} = T_{h,lay3}; T_{heat,in} = T_{h,lay1} \quad (35)$$

The operating parameters are shown in Table 3. The initial conditions for the hot and cold storage units and the metal plate of the solar collector, respectively, are:

$$\begin{aligned} T_{h,lay,1} &= T_{h,lay,2} = T_{h,lay,3} = 60^\circ\text{C}; \quad T_{clay,1} = T_{clay,2} = T_{clay,3} = 10^\circ\text{C}; \\ T_{fp}|_{t=\text{start}} &= T_{Amb}|_{t=\text{start}} \end{aligned} \quad (6)$$

These are the initial conditions at time $t = 0$, when the whole simulation begins. The values for the initial conditions at the moment when the components are enabled on subsequent days differ from the previous values for the first day because during the night a subset of equations continues to be solved to take the heat losses into account. These losses are calculated for all the components except the chiller, which is assumed to be perfectly insulated. The post-heating valve control relies on a trend proportional to the

adiabatic mixing temperature. The flow sent to the post-heating section and the boiler operating curve comply with:

$$\begin{cases} \dot{m}_{ph,in} = \dot{m}_{ph} & T_{[4]} < T_{inf} \\ \dot{m}_{ph,in} = \dot{m}_{ph} \left(\frac{T_{sup} - T_{[4]}}{T_{sup} - T_{inf}} \right) & T_{inf} < T_{[4]} < T_{sup} \\ \dot{m}_{ph,in} = 0 & T_{[4]} > T_{sup} \end{cases} \quad (7)$$

$$\begin{cases} Q_{boiler} = P_{boiler} \dots \dots \dots \text{if } T_{boiler,in} < T_{setboiler,min} \\ Q_{boiler} = \frac{P_{boiler}(T_{setboiler,max} - T_{boiler,in})}{T_{setboiler,max} - T_{setboiler,min}} \dots \dots \dots \\ \dots \dots \dots \text{if } T_{setboiler,min} < T_{boiler,in} < T_{setboiler,max} \\ Q_{boiler} = 0 \dots \dots \dots \text{if } T_{boiler,in} > T_{setboiler,max} \end{cases} \quad (8)$$

The mathematical model was developed entirely with Matlab/Simulink® 7.6.0 using a block programming approach. The model's graphical interface is shown in Fig. 4. The differential-algebraic equations were solved numerically with a second-order modified Rosenbrock solution method named ode23s.

6. Evaluation of the performance

The chiller's cooling power is calculated by:

$$Q_{cooling} = \dot{m}_{cool} c_{pw} (T_{ev,in} - T_{ev,out}) \quad (36)$$

The heating power in the packed beds exchangers is:

$$Q_{heat} = \dot{m}_{heat} c_{pw} (T_{heat,out} - T_{heat,in}) \quad (37)$$

The condensing power is expressed as:

$$Q_{cond} = (\dot{m}_{cond,ex} + \dot{m}_{z,ex}) c_{pw} (T_{dry,out} - T_{dry,in}) \quad (38)$$

The COP and the SPC are:

$$COP = \frac{Q_{cooling}}{Q_{heat}} \quad (39)$$

$$SCP = \frac{Q_{cooling}}{2M_z} \quad (40)$$

For the boiler, the actual thermal power of the heat generator is calculated as:

$$Q_{boiler} = (\dot{m}_{boiler} + \dot{m}_{ph}) c_{pw} (T_{boiler,out} - T_{boiler,in}) \quad (41)$$

The natural gas consumption in the boiler during the simulation time is:

$$V_{NG} = \int_{0s}^{\text{end time sim.}} \frac{Q_{boiler}}{Q_{cal,NG}} dt \quad (42)$$

where V_{NG} are the cubic meters of natural gas consumption in standard conditions and $Q_{cal,NG}$ is the natural gas calorific value, assumed to be 39835.4 kJ/m³.

The total incident radiation is:

$$I_{inc} = I_{tilt} A_{coll} \quad (43)$$

The heating power absorbed by the solar field is:

$$I_{abs} = \dot{m}_{solar} c_{pw} (T_{solcol,out} - T_{solcol,in}) \quad (44)$$

Table 3
Parameters of the differential-algebraic system.

A_{coll}	40	m ²
$A_{drycool}$	40	m ²
A_{fp}	90	m ²
A_{fpamb}	40	m ²
$A_{ph,ex}$	10	m ²
$A_{c,lay1/2/3}$	1	m ²
$A_{h,lay1/2/3}$	1	m ²
$A_{c,lay}$	0.1	m ²
$A_{h,lay}$	0.5	m ²
$A_{stsolcolex}$	10	m ²
BP	0.3	
M_{fp}	900	kg
P_{boiler}	24	kW
RF	0.9	
$U_{drycool}$	80	W/(m ² K)
U_{fp}	500	W/(m ² K)
$U_{fp,amb}$	1.5	W/(m ² K)
$U_{ph,ex}$	80	W/(m ² K)
U_{coldst}	0.6	W/(m ² K)
U_{hotst}	0.6	W/(m ² K)
$U_{stsolcol,ex}$	200	W/(m ² K)
U_w	10	W/(m ² K)
$V_{c,lay1/2/3}$	0.3	m ³
$V_{h,lay1/2/3}$	0.8	m ³
ϵ	0.9	
$\dot{m}_{air,day}$	0.3	kg/s
\dot{m}_{boiler}	1	kg/s
\dot{m}_{heat}	2	kg/s
\dot{m}_{ph}	0.1	kg/s
\dot{m}_{ref}	1.5	kg/s
\dot{m}_{solar}	10	kg/s
$(\tau a)_{eff}$	0.8	
T_{inf}	16	°C
T_{sup}	19	°C
$T_{set \text{ boiler,MAX}}$	80	°C
$T_{set \text{ boiler,min}}$	50	°C
$A_{cond,ex}$	10	m ² [15]
$A_{ev,ex}$	10	m ² [15]
$A_{z,ex}$	40	m ² [15]
c_z	950	J/(kg K)
$M_{cond,ex}$	5	kg [15]
$M_{ev,ex}$	5	kg [25]
$M_{z,ex}$	5	kg (assumed)
M_z	30	kg [9]
$U_{cond,ex}$	600	W/(m ² K) [26]
$U_{ev,ex}$	600	W/(m ² K) (assumed)
$U_{z,ex}$	50	W/(m ² K) [15]
$\dot{m}_{z,ex}$	0.43	kg/s
$\dot{m}_{cond,ex}$	2	kg/s
$\dot{m}_{ev,ex}$	1	kg/s
$t_{end,1/3}$	150	sec
$t_{end,2/4}$	600	sec
$\Delta T_{inf/sup}$	20	°C

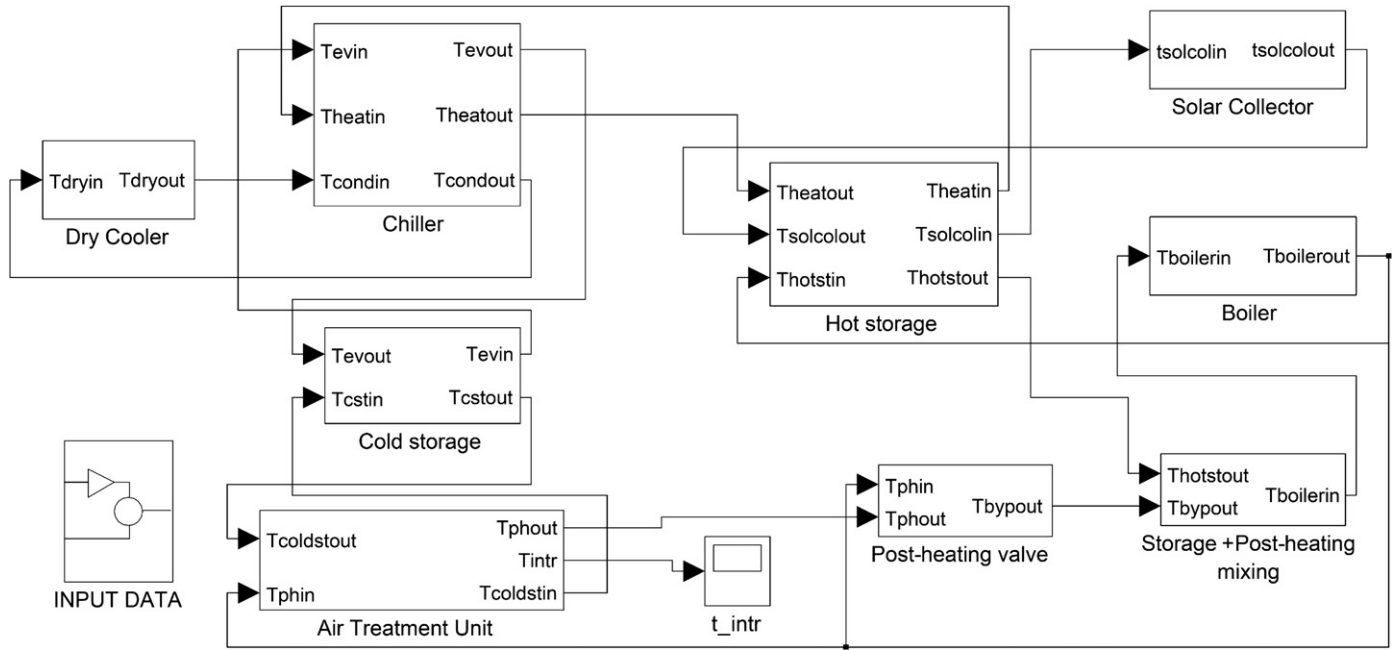


Fig. 4. Matlab/Simulink® model of the system.

7. Results

7.1. Time-dependent patterns

The main results are presented below studying the transients of several quantities on the second day simulated. Only the second day was considered because the results obtained on the first are usually influenced by the initial conditions adopted. The patterns of the main chiller variables are quite similar to those previously reported in the literature [19,20]. The novel aspect of present work consists in the ability to follow the adsorption machine end-phases relating to the bed thermodynamics, which were not considered in previous transient models covering some consecutive days. Fig. 5 shows the effect of the variable radiation on the trend of the maximum bed temperatures in each cycle. The values of T_z for beds 1 and 2 (T_{z1} , T_{z2}) vary from 29.2 °C to 59.8 °C. The temperature $T_{heat,in}$ at the inlet to the heat exchangers of the adsorbent beds varies within a range of approximately 18 °C throughout the day. The temperatures at the inlet and outlet of the chiller's cooling circuit (T_{ev} , $T_{ev,ex}$, $T_{ev,out}$) follow the same qualitative trends but with an average temperature difference of approximately 1 °C. For the condenser circuit, the temperatures $T_{dry,in}$ and $T_{dry,out}$ are very similar, differing from T_c by about 0.5 °C.

Looking at the maximum peaks of $T_{heat,in}$, T_{z1} , T_{z2} we see that the maximum value for $T_{heat,in}$ of 69.8 °C occurs at 14.0 h, while the peaks for T_{z1} and T_{z2} are quite similar and amount to 59.7 °C, obtained at 14.2 h and 14.0, revealing a delay of 12 min for bed 1. The minimum value of $T_{ev,out}$ was 8.0 °C. Considering a single cycle of one of the beds, the change in uptake is of the order of 4%, due to the low regeneration temperatures. Similar result was found in [21,22]. Fig. 5 shows also the trends of the temperatures of the solar energy collection subsystem. As concerns the hot storage unit, the temperatures of the three layers follow the same trends. The hot storage unit's average temperature is 64.4 °C, with a maximum of 76.9 °C in layer 1 and a minimum of 57.1 °C in layer 3. The metal plate inside the solar collector and the carrier fluid leaving the collector have very similar temperatures. Neglecting the first hours trend, the maximum peak for T_{fp} is 82.9 °C at 13.3 h, while the maximum for $T_{h,lay1}$ corresponding to 69.8 °C occurs at 14.03.

Fig. 6 shows the trend of the ambient temperature (between 24 °C and 27 °C during the system's operation), of the air temperatures after adiabatic mixing $T_{[4]}$ and at the user $T_{[5]}$ and of the temperatures of the three layers in the cold storage unit. The trend of the ambient relative humidity is also shown. The temperatures of the three layers of the cold storage unit vary between 8.6 °C and 10.9 °C, with negligible differences (below 0.5 °C) among layers. The treated air temperature $T_{[5]}$ ranged between 16.1 °C and 17.2 °C.

Fig. 7 shows that the peak incident radiation is 36.2 kW, while the peak absorbed power is 25.7 kW. The boiler's maximum capacity is 19.4 kW and its daily consumption of natural gas is 12.6 Nm³. The SCP, disregarding the start-up transient, averages 69.3 W/kg. The cooling power Q_{cool} is stable and acquires a mean value of 4.1 kW. The heating power of the two adsorbent beds Q_{heat} has a mean value of approximately 24.7 kW and the condensing power has a mean value of around 9.2 kW.

Fig. 8 shows the instantaneous COP and the COP of every cycles. The daily average is 0.18, changing instantaneously between 0.04 and 0.3. The COP of the single cycle at the time of starting up the plant is just below 0.3, then drops and settles for most of the period of operation at around 0.2, ranging between 0.15 and 0.25. In the final hours of operation of the chiller, there is a rising trend of the COP because the cooling power remains at the same levels as during the previous hours, but the heat coming from the heating section of the system decreases as the radiation decreases. The results from this base case are consistent with the literature in the COP [9,22–24] but the plant efficiency is not optimized. Therefore it is necessary a further analysis to identify a reduced number of operational parameters which are most influencing the performance of the whole solar cooling system and each its subsystem.

7.2. Spectral analysis

The study of the variables transient can be simplified regressing them with Fourier series. Such regression demands a preliminary understanding of the main frequencies characterizing the variable being investigated. This approach is commonly applied to signal analysis, but can prove useful for analyzing the results of the present model too. Using the Fast Fourier Transform of the variables

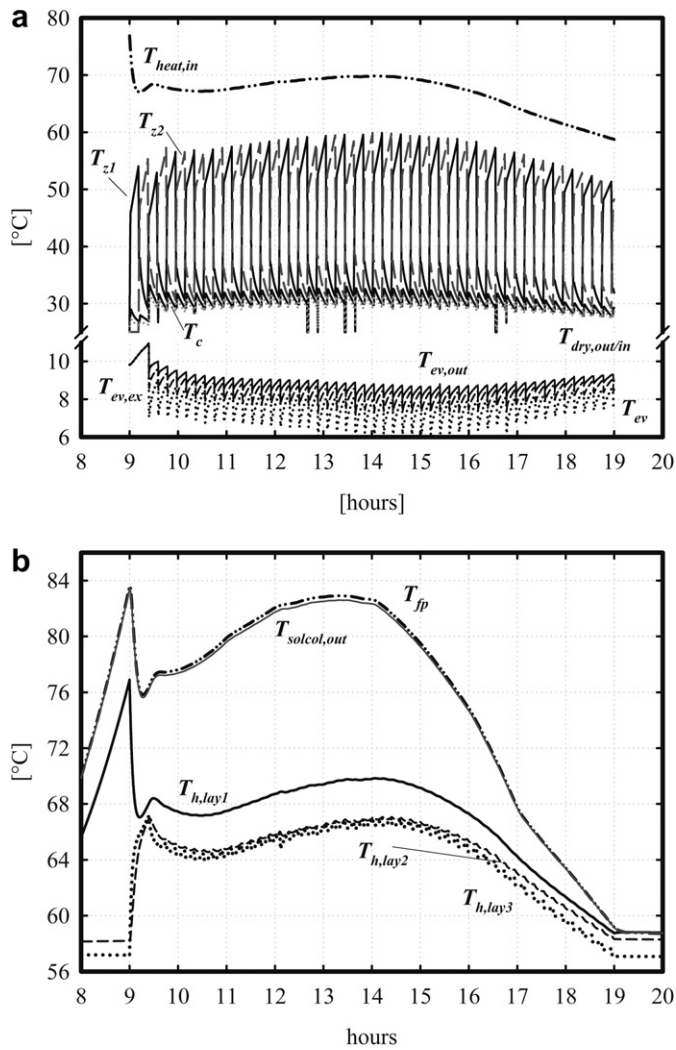


Fig. 5. (a) Temperatures relating to the chiller's operation and (b) temperatures relating to the solar energy collection sub-system.

enables us to know the most important frequencies comprising each signal. Fig. 9 shows the normalized periodograms of the most important temperatures, powers and climate data characterizing the adsorption chiller's operation and the COP. It is evident that the

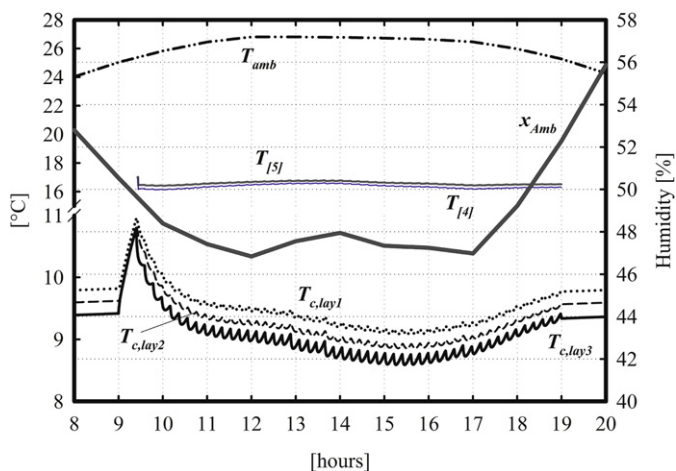


Fig. 6. Temperatures and relative humidity relating to the air treatment unit.

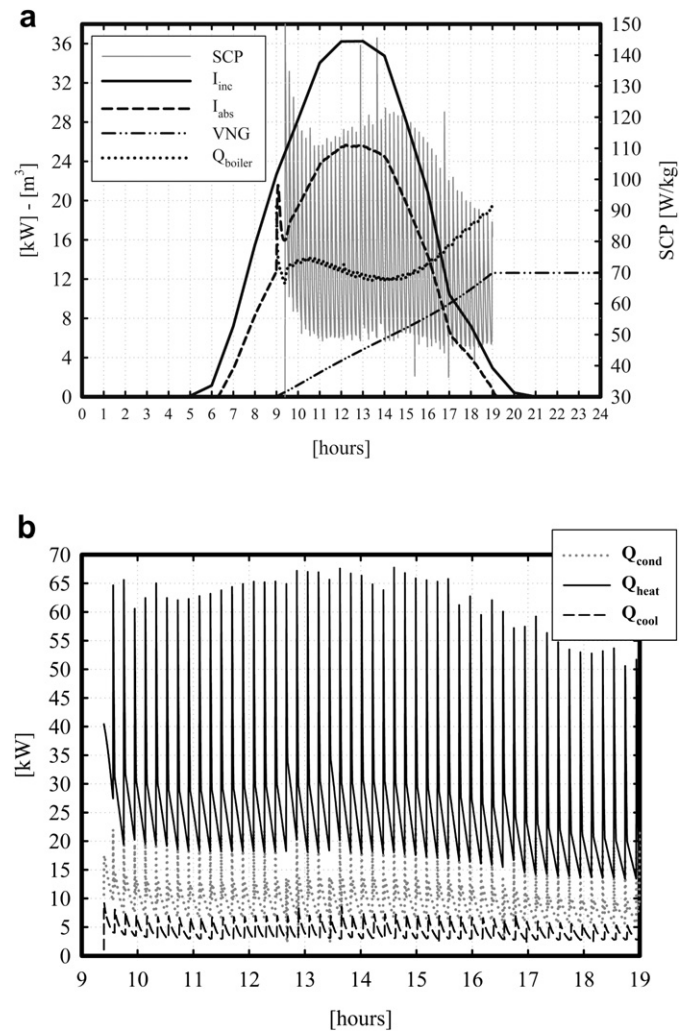


Fig. 7. (a) The power and performance of the main subsystems in the plant (b) powers relating to the adsorption chiller's operation.

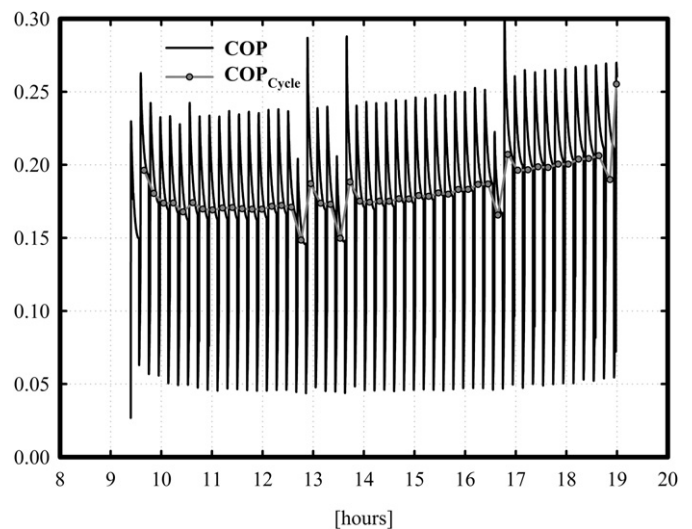


Fig. 8. Instantaneous COP and COP of each cycle (calculated over the cycle time) of the adsorptive chiller.

transient of these quantities is described by a limited number of fundamental frequencies. For some variables and for the input climate data the important frequencies are lying below 1 cycle/hour, even though $T_{c,lay3}$ has a negligible component around 5 cycles/hour as visible also in Fig. 6.

The correlation between the signals is present when the peaks have the same or multiple frequencies. The frequency-based analysis also enables us to see which frequencies are most important for reconstructing the signal. In particular, the climate data and the variables relating to the subsystems other than the adsorption chiller are dominated by low frequencies, whereas the variables relating to the adsorption chiller's operation also involve high frequencies. So uncoupling the low frequencies bands (typical of climate data) composing a signal and the high frequencies bands composing the same signal (typical of the logic involved in controlling the solar cooling system and the adsorption chiller), it is possible to highlight the correlation between the signals.

7.3. Cross-correlations

Performing the discrete Fourier cosine transforms of the chiller operating variables and considering only the first 20 modes enables the high-frequency trends to be omitted, so that we can concentrate on the lower frequencies alone. Fig. 10 shows the regressions of several chiller operating variables, considering only the first 20 modes.

Fig. 11 shows the cross-correlation between the most important operating parameters considering only the first 20 modes for the chiller operating variables, and the original signal for T_{Amb} and the sum of Radiation + Q_{boiler} (the thermal power released to the hot storage unit). A study of the cross-correlations between the signals

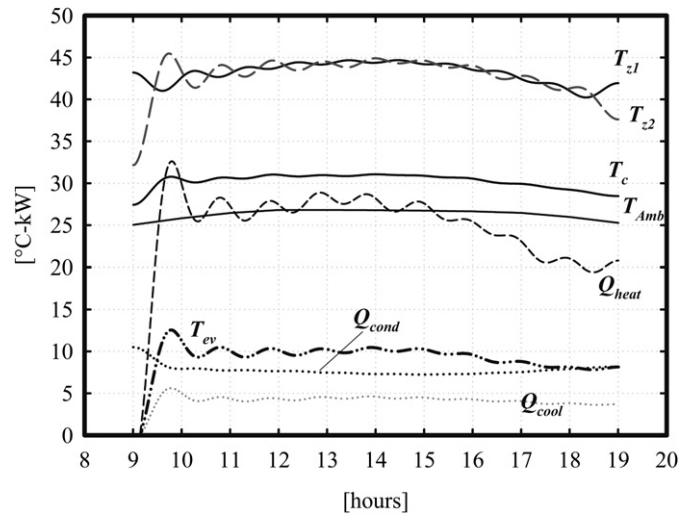


Fig. 10. Discrete cosine transforms of the chiller's operating variables at low frequencies (considering just the first 20 modes).

clearly shows any correlations, even if they have a phase shift. Cross-correlation also enables the correlations to be arranged from the most to the least important and lets us establish whether the correlation is direct or inverse.

Cross-correlating the COP with the other chiller operating variables enables us to see which variables have the greatest influence on the COP, and how much they influence the latter. Applying the cross-correlation to the climate data enables us to see

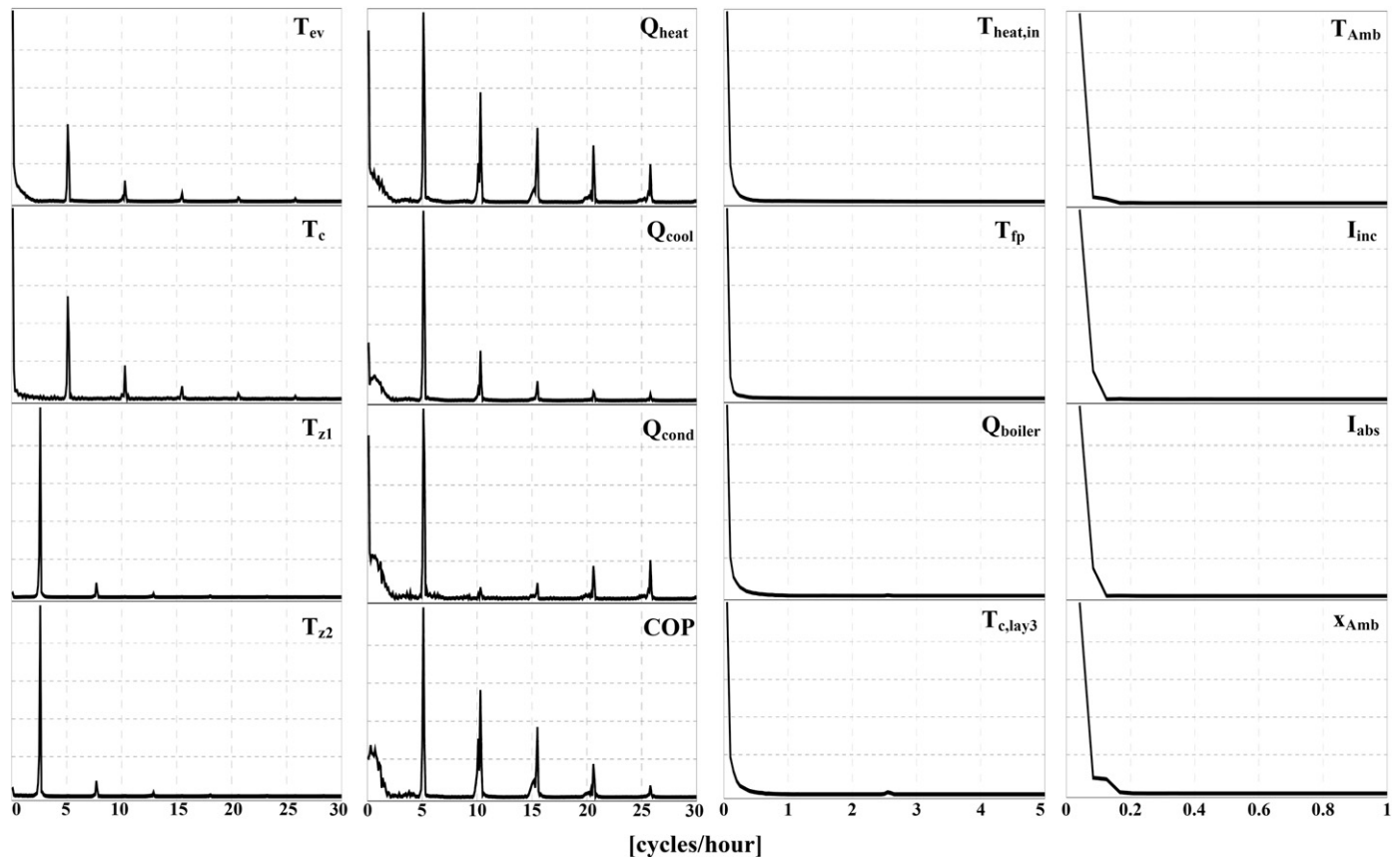


Fig. 9. Periodograms of some variables involved in the solar cooling system operation.

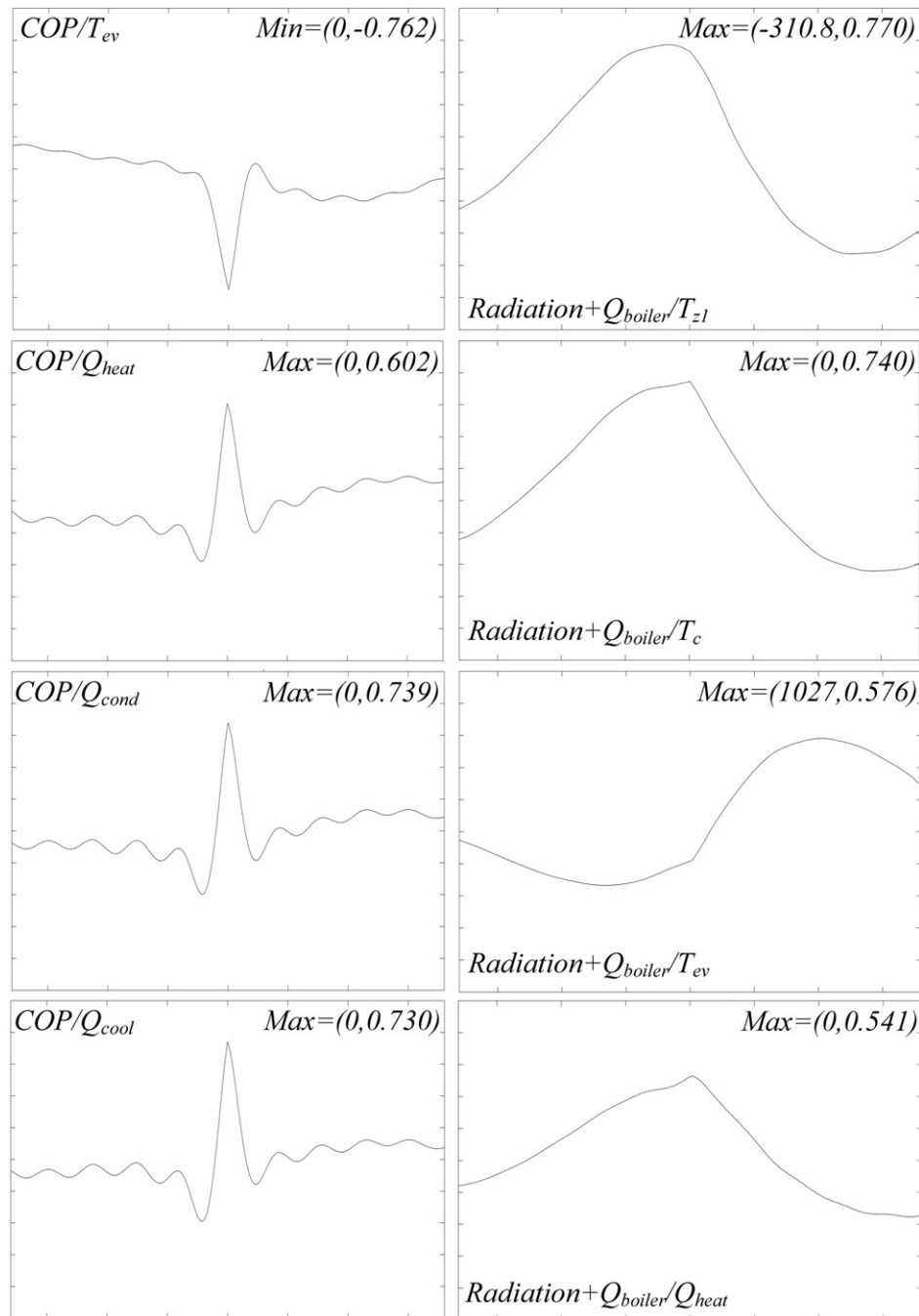


Fig. 11. Selected cross-correlations of the operating variables for the solar cooling system.

which variables are affected by variations in climate data, and to what degree they are affected. In the following analysis, only the values outside the range of ± 0.500 were considered significant. The cross-correlations identified the following influences (listed in order of importance and as absolute values).

- 1) $COP = f(T_{ev}, Q_{cond}, Q_{cool}, Q_{heat})$ with $T_{ev} > Q_{cond} > Q_{cool} > Q_{heat}$. This means that when the COP increases, then T_{ev} decreases, while Q_{cool} , Q_{cond} and Q_{heat} increase. To maximize the COP, we therefore need to take the following steps, in order of priority: i) to always ensure an accurate condensation; ii) to pay attention to the design of the evaporator and iii) to use high flow rates and heat exchange surface areas for the adsorbent beds.

- 2) The thermal power delivered to the hot storage unit ($Radiation + Q_{boiler}$) is correlated with $(T_{z1}, T_c, T_{ev}, Q_{heat})$, where $T_{z1} > T_c > T_{ev} > Q_{heat}$, but T_{ev} and Q_{heat} have cross-correlation coefficients below 0.6, so the correlation is less important. T_{z1} and T_{ev} have a phase shift of 53 min and 2.85 h, respectively, due to inertias in the solar cooling system. T_c is influenced by $Radiation + Q_{boiler}$ because the radiation correlates strongly with the ambient temperature.

8. Conclusions

A dynamic multi-level mathematical model was developed to study the operation of a two bed silica gel-water adsorption chiller

for solar cooling applications. Variable temperature, humidity and solar radiation conditions were taken into account. The model provides accurate results for use in the further optimization and investigation of the system as a whole, the subsystems and the chiller. The operating transients of the system can be tracked from start-up to shut-down on any given day of operation. The model was verified on a baseline case and the results were in the form of arrays of time-dependent values.

The obtained results are consistent with the previous models in literature. The results show that the solar cooling system can be further optimized, but a preliminary identification of the correlations among the variables influencing the performance of the solar cooling system and its subsystems have to be performed. The cross-correlations of the variables allow to select a reduced numbers of them for the optimization. The main result from the model is the obtained classification of importance among the variables in the transients. Hence the model enables a sensitivity analysis on the most influential parameters for some interesting outputs. Conclusions can be drawn on the basis of these results on the most appropriate control strategy and on the response of the adsorption chiller over a lengthy operational period. A spectral analysis was proposed on these data for identification of the correlation among the variables involved in the solar cooling system in order to study the effects of the input parameters on the outputs. Concentrating the study just a limited number of variables describing the chiller operation, the outcomes highlight that the COP depends mainly on $T_{ev} > Q_{cond} > Q_{cool} > Q_{heat}$ and the thermal power Radiation + Q_{boiler} influences $T_{z1} > T_c > T_{ev} > Q_{heat}$.

Appendix

- The adsorbent/adsorbate equilibrium was calculated as:

$$\ln p_z = A_z(w) + \frac{B_z(w)}{T_z} \quad (A.1)$$

where $A_z(w)$ and $B_z(w)$ are polynomials with coefficients determined experimentally at the CNR-ITAE laboratories ($a_0 = 12.17$; $a_1 = 1.495$; $a_2 = -0.07295$; $a_3 = 0.00107$; $b_0 = -4178$; $b_1 = -312.3$; $b_2 = 16.78$; $b_3 = -0.2501$)

- The adsorption/desorption enthalpy $\Delta H_{ads}(w)$ was calculated as:

$$\Delta H_{ads}(w) = -B_z(w) \frac{R}{M_g} \quad (A.2)$$

where R is the universal gas constant and M_g is the molecular mass of the water.

References

- [1] Critoph RE. Rapid cycling solar/biomass powered adsorption refrigeration system. *Renewable Energy* 1999;16:673–8.
- [2] Critoph RE, Metcalf SJ, Tamainot-Telto Z. Proof of concept car adsorption air conditioning system using a compact sorption reactor. *Heat Transfer Eng* 2010;31:950–6.
- [3] Nunez T, Mittelbach W, Henning HM. Development of an adsorption chiller and heat pump for domestic heating and air-conditioning applications. *Appl Therm Eng* 2007;27:2205–12.
- [4] Jacob U. Performance analysis of small-scale sorption chillers, innovative materials for processes in energy systems 2010 (IMPRES), CD- Proceedings ISBN 978-981-08-7614-2, (2010) 238–244. doi:10.3850/978-981-08-7614-2 IMPRES063.
- [5] Schicktzan M, Nunez T. Modelling of an adsorption chiller for dynamic system simulation. *Int J Refrig* 2009;32:588–95.
- [6] Saha BB, Akisawa A, Kashiwagi T. Solar/waste heat driven two-stage adsorption chiller: the prototype. *Renewable Energy* 2001;23:93–101.

- [7] Saha BB, Koyama S, Ng KC, Hamamoto Y, Akisawa A, Kashiwagi T. Study on a dual-mode, multi-stage, multi-bed regenerative adsorption chiller. *Renewable Energy* 2006;31:2076–90.
- [8] Wang DC, Wang YJ, Zhang JP, Tian XL, Wu JY. Experimental study of adsorption chiller driven by variable heat source. *Energy Convers Manage* 2008;49:1063–73.
- [9] Chang WS, Wang CC, Shieh CC. Design and performance of a solar-powered heating and cooling system using silica gel/water adsorption chiller. *Appl Therm Eng* 2009;29:2100–5.
- [10] Di J, Wu JY, Xia ZZ, Wang RZ. Theoretical and experimental study on characteristics of a novel silica gel-water chiller under the conditions of variable heat source temperature. *Int J Refrig* 2007;30:515–26.
- [11] Wu JY, Li S. Study on cyclic characteristics of silica gel/water adsorption cooling system driven by variable heat source. *Energy* 2009;34:1955–62.
- [12] Luo H, Wang R, Dai Y. The effects of operation parameter on the performance of a solar powered adsorption chiller. *Appl Energy* 2010;87:3018–22.
- [13] Chua HT, Ng KC, Wang W, Yap C, Wang XL. Transient modeling of a two-bed silica gel-water adsorption chiller. *Int J Heat Mass Transfer* 2004;47:659–69.
- [14] Kreft JGG, de Leeuw J. *Introducing multilevel modeling*. 1st ed. London: Sage Publications Ltd; 1998.
- [15] Sapienza A, Vasta S, Freni A, Restuccia G. Design and operation of a new adsorption chiller prototype driven by low grade thermal energy, 3rd International Conference Solar Air-Conditioning Conference, Palermo, Italy. CD- Proceedings ISBN 978-3-941785-06-9, Paper ID 024, (2009) 6 pages.
- [16] Muneer T. *Solar radiation and daylight models*. 2nd ed. Linacre House, Jordan Hill, Oxford OX2 8DP, 200 Wheeler Road, Burlington, MA 01803: Elsevier Butterworth-Heinemann; 2004.
- [17] Khan MZI, Saha BB, Alam KCA, Akisawa A, Kashiwagi T. Study on solar/waste heat driven multi-bed adsorption chiller with mass recovery. *Renewable Energy* 2007;32:365–81.
- [18] Khan MZI, Alam KCA, Saha BB, Akisawa A, Kashiwagi T. Performance evaluation of multi-stage, multi-bed adsorption chiller employing re-heat scheme. *Renewable Energy* 2008;33:88–98.
- [19] Clausse M, Alam KCA, Meunier F. Residential air conditioning and heating by means of enhanced solar collectors coupled to an adsorption system. *Solar Energy* 2008;82:885–92.
- [20] Wang X, Chua HT. Two bed silica gel-water adsorption chillers: an effectual lumped parameter model. *Int J Refrig* 2007;30:1417–26.
- [21] Chua HT, Ng KC, Malek A, Kashiwagi T, Akisawa A, Saha BB. Modeling the performance of two-bed, silica gel-water adsorption chillers. *Int J Refrig* 1999;22:194–204.
- [22] Chen CJ, Wang RZ, Xia ZZ, Kiplagat JK. Study on a silica gel-water adsorption chiller integrated with a closed wet cooling tower. *Int J Therm Sci* 2010;49:611–20.
- [23] Saha BB, Boelman EC, Kashiwagi T. Computational analysis of an advanced adsorption-refrigeration cycle. *Energy* 1995;20:983–94.
- [24] Luo HL, Dai YJ, Wang RZ, Wu JY, Xu YX, Shen JM. Experimental investigation of a solar adsorption chiller used for grain depot cooling. *Appl Therm Eng* 2006;26:1218–25.
- [25] Chen CJ, Wang RZ, Xia ZZ, Kiplagat JK, Lu ZS. Study on a compact silica gel-water adsorption chiller without vacuum valves: design and experimental study. *Appl Energy* 2010;87:2673–81.
- [26] Loh WS, Saha BB, Chakraborty A, Ng KC, Chun WG. Performance analysis of waste heat driven pressurized adsorption chiller. *J Therm Sci Technol* 2010;5:252–65.

Nomenclature

Symbols

- A_{coll} : active surface of the solar field; m²
 BP : by-pass factor (range 0–1)
 COP : coefficient of performance
 c_{pa} : specific heat of air; J/(kg K)
 c_{pw} : specific heat of water; J/(kg K)
 H : enthalpy of the moisture, J/kg
 I_{tilt} : solar radiation on collector with β tilt angle (30°); W/m²
 L_w : heat of water evaporation; J/kg
 $\dot{m}_{air,day/night}$: air mass flow circulating in the ATU with the system enabled during the day/night; kg/s
 \dot{m}_{boiler} : water mass flow rate in the boiler; kg/s
 \dot{m}_{BP} : by-passing air mass flow rate ($\dot{m}_{BP} = BP \dot{m}_{air,day}$); kg/s
 \dot{m}_{cond} : mass flow rate of the water circulating in the condenser of the adsorption chiller; kg/s
 $\dot{m}_{cond,ex}$: mass flow rate of the water circulating in the dry cooler; kg/s
 $\dot{m}_{ev,ex}$: mass flow rate of the water circulating in the refrigeration loop; kg/s
 \dot{m}_{heat} : mass flow rate of the hot water delivered to the adsorption chiller; kg/s
 \dot{m}_{ph} : mass flow rate of the water for post-heating exchanger upstream from the reg. valve; kg/s
 $\dot{m}_{ph,in}$: mass flow rate of the water in the post-heating exchanger; kg/s
 \dot{m}_{ref} : mass flow rate of the water circulating between the cold storage unit and ATU; kg/s
 \dot{m}_{solar} : mass flow rate of the water in the solar loop; kg/s
 \dot{m}_{tr} : mass flow rate of the air in contact with heat exchanger ($\dot{m}_{tr} = (1 - BP) \dot{m}_{air,day}$); kg/s

$\dot{m}_{z,ex}$: mass flow rate of the water in the packed bed heat exchanger for the cooling phases; kg/s

P_{boiler} : rated thermal power of the boiler; kW

Q_{boiler} : actual heating power generated by the boiler; W

$Q_{cooling}$: cooling power generated by the chiller; W

Q_{heat} : heating power used by the chiller; W

Q_{cond} : condensation power of the chiller; W

r : heat of water condensation, J/kg

RF : ambient thermal factor

RH : relative humidity, %

SCP : specific cooling power; W/(kg of adsorbent)

$T_{inf/sup}$: min./max. control temperature of the reg. valve for the post-heating exchanger, °C

$T_{setboiler,min/max}$: min./max. set point temperature of the boiler, °C

U : overall heat transfer coefficient, W/(m² K)

U_{coldst} : overall heat transfer coefficient between cold storage unit and environment, W/(m² K)

U_{hotst} : overall heat transfer coefficient between hot storage unit and environment, W/(m² K)

U_w : overall heat transfer coefficient between two layers in the storage units, W/(m² K)

x : specific humidity; g/kg

w : uptake; %

Greek letters

ρ_w : water density, kg/m³

ΔH : adsorption enthalpy; J/kg

ΔT_{lm} : logarithmic mean temperature difference; °C

ϵ : efficiency of cooling and dehumidifying exchanger

$(\tau\alpha)_{eff}$: effective absorption transmissibility coefficient

Subscripts

ads : adsorption (in ΔH_{ads})

Amb : ambient

byp,out : outlet of the tee between the post-heating outlet and the byp. valve (in $T_{byp,out}$)

$boiler,in/out$: boiler inlet/outlet (in $T_{boiler,in}$, $T_{boiler,out}$)

BP : by-passed (in \dot{m}_{BP})

c : condensation (in T_c)

$cond,ex$: of the condensation heat exchanger (in $T_{cond,ex}$, $M_{cond,ex}$, $A_{cond,ex}$, $U_{cond,ex}$)

$cond,in/out$: of the chiller's condensation loop inlet/outlet (in $T_{cond,in}$, $T_{cond,out}$)

c,lay : between the layers in the cold storage unit (in $A_{c,lay}$)

$c,lay1/2/3$: layer 1/2/3 of the cold storage unit (in $T_{c,lay1}$, $A_{c,lay1}$, $V_{c,lay1}$, $T_{c,lay2}$, $A_{c,lay2}$, $V_{c,lay2}$, $T_{c,lay3}$, $A_{c,lay3}$, $V_{c,lay3}$)

$coldst,in/out$: cold storage unit inlet/outlet (in $T_{coldst,in}$, $T_{coldst,out}$)

$coldst,pc$: in the post-cooling state (in $T_{coldst,pc}$)

dry : dry cooler (in U_{dry} , A_{dry})

$dry,in/out$: condenser inlet/outlet (in $T_{dry,in}$, $T_{dry,out}$)

ev : evaporation (in T_{ev})

ev,ex : of the evaporation heat exchanger (in $T_{ev,ex}$, $M_{ev,ex}$, $A_{ev,ex}$, $U_{ev,ex}$)

$ev,in/out$: of the chiller's refrigeration loop inlet/outlet (in $T_{ev,in}$, $T_{ev,out}$)

fp : metal plate of the solar collectors (in T_{fp} , A_{fp} , U_{fp})

$heat,in/out$: bed exchanger inlet/outlet (in $T_{heat,in}$, $T_{heat,out}$)

h,lay : between the layers of the hot storage unit (in $A_{h,lay}$)

$h,lay1/2/3$: layer 1/2/3 of the hot storage unit (in $T_{h,lay1}$, $A_{h,lay1}$, $V_{h,lay1}$, $T_{h,lay2}$, $A_{h,lay2}$, $V_{h,lay2}$, $T_{h,lay3}$, $A_{h,lay3}$, $V_{h,lay3}$)

$hotst,in/out$: hot storage unit inlet/outlet (in $T_{hotst,in}$, $T_{hotst,out}$)

lm,ph : logarithmic mean in the post-heating exchanger (in $\Delta T_{lm,ph}$)

ph,ex : post-heating exchanger (in $U_{ph,ex}$, $A_{ph,ex}$)

$ph,in/out$: post-heating exchanger inlet/outlet (in $T_{ph,in}$, $T_{ph,out}$)

$stsolcol,ex$: heat exchanger in the hot storage unit of the solar field (in $U_{stsolcol,ex}$, $A_{stsolcol,ex}$)

$solcol,in/out$: inlet/outlet of the solar collector (in $T_{solcol,in}$, $T_{solcol,out}$)

tr : treated (in \dot{m}_{tr})

w : water (in ρ_w , U_w)

z : of the adsorbent material (in T_z , M_z , c_z)

z,ex : of the heat exchanger in the adsorbent bed (in $c_{z,ex}$, $U_{z,ex}$, $A_{z,ex}$)

[1]: ambient air intake condition (in $T_{[1]}$, $x_{[1]}$)

[2]: air in the cooling battery with no dehumidification (in $T_{[2]}$, $x_{[2]}$)

[R]: dew point condition (in $T_{[R]}$, $x_{[R]}$)

[3]: treated air downstream from the cooling and dehumidification (in $T_{[3]}$, $x_{[3]}$)

[4]: condition of air after adiabatic mixing (in $T_{[4]}$, $x_{[4]}$)

[5]: condition of air flowing to the user (in $T_{[5]}$, $x_{[5]}$)